buildings

MDPI

Article

Performance Optimization of Flood Sediment Adobe Bricks Through Natural Additive Integration

Andaman Khunaprapakorn [1], Rungroj Arjwech [2], Natthaphol Chomsaeng [3] and Sitthiphat Eua-Apiwatch [4,*]

[1] Shrewsbury International School Bangkok Riverside, Bangkok 10120, Thailand; 2026anda.k@shrewsbury.in.th
[2] Department of Geotechnology, Faculty of Technology, Khon Kaen University, Khon Kaen 40002, Thailand; rungroj@kku.ac.th
[3] Department of Advanced Materials Engineering, Faculty of Engineering, Burapha University, Saen Suk 20131, Thailand; natthaphol@eng.buu.ac.th
[4] Department of Civil Engineering, Faculty of Engineering, Burapha University, Saen Suk 20131, Thailand
* Correspondence: sitthiphat@eng.buu.ac.th

Abstract

This study addresses critical knowledge gaps in adobe construction by systematically investigating soil mineralogy–additive effectiveness relationships and developing dual-additive optimization strategies for flood sediment valorization. Four Thai soil types—Nakhon Pathom (NPT), Sisaket (SSK), Uttaradit (UTT), and September 2024 Chiang Rai flood sediment (CRI)—were characterized using XRD and EDS analyses. Twelve adobe formulations incorporating rice husk (3.45%) and graduated bentonite concentrations (5–15%) were evaluated for mechanical and thermal properties. UTT soil with balanced mineralogy (42.1% SiO_2, 40.4% Al_2O_3) achieved optimal mechanical performance (3.12 ± 0.11 MPa compressive strength), while CRI demonstrated superior thermal insulation (0.200 ± 0.009 W/m·K). Rice husk systematically enhanced compressive strength across all soils (13.6–82.5% improvement) while reducing thermal conductivity to 0.211–0.278 W/m·K. Dual-additive optimization of CRI enabled application-specific customization: rice husk alone maximized strength (1.34 ± 0.09 MPa), while bentonite combinations optimized thermal performance (0.199 ± 0.015 W/m·K). Microstructural analysis revealed distinct reinforcement mechanisms and matrix densification effects. This research establishes predictive frameworks for material selection based on soil composition, demonstrates viable flood waste valorization pathways, and supports Thailand's Bio-Circular-Green economic framework through sustainable construction material development.

Keywords: adobe bricks; rice husk; sodium bentonite; flood sediment

Academic Editor: Biao Hu

Received: 29 August 2025
Revised: 23 September 2025
Accepted: 26 September 2025
Published: 28 September 2025

Citation: Khunaprapakorn, A.; Arjwech, R.; Chomsaeng, N.; Eua-Apiwatch, S. Performance Optimization of Flood Sediment Adobe Bricks Through Natural Additive Integration. *Buildings* **2025**, *15*, 3508. https://doi.org/10.3390/buildings15193508

1. Introduction

Adobe construction is increasingly valued for its low environmental footprint, affordability, and compatibility with vernacular building traditions, particularly in rural or low-income contexts [1]. Adobe materials offer significant environmental advantages, with CO_2 emissions of 22 kg/ton compared to the 143 kg/ton of concrete blocks [1]. Recent studies have emphasized the role of circular economy strategies in adobe construction, demonstrating how waste valorization contributes to reducing embodied emissions [2]. However, conventional adobe bricks are limited by their structural and thermal properties, with compressive strength values significantly varying between manufacturers and manufacturing techniques [3,4]. Hence, additional enhancements are required for adobe bricks to become suitable for modern energy-efficient applications.

Efforts to enhance the performance of Adobe bricks have focused on the incorporation of organic fibers and natural clay minerals. Natural fiber reinforcement has demonstrated significant potential across diverse geographical contexts, with various plant-based fibers achieving substantial mechanical improvements [5–7]. Parallel advances in geopolymer and fiber-reinforced bricks further illustrate how natural fibers and alternative binders can enhance both thermal and mechanical performance [8]. For instance, studies on seagrass fibers (Posidonia Oceanica) have shown superior performance to straw, confirming the potential of alternative natural fibers [9].

Rice husk, a widely available agricultural by-product in Thailand, containing 45% cellulose, 19% hemicelluloses, 19.5% lignin, and 15% silica by weight [10], has been shown to improve adobe brick properties when incorporated into mixtures, though the effects vary with soil composition and require optimization [11]. Research in Thailand has demonstrated that while the addition of rice husk significantly improves shrinkage resistance and provides important reinforcement benefits, it can reduce compressive strength [11]. Other studies have found considerable improvements in the properties of adobe composites reinforced with other natural fibers. An example is the palm-fiber reinforcement, which is linked to a 59% increase in compressive strength of adobe bricks [12]; sisal-fiber reinforcement shows a 240% increase in compressive strength at optimal concentrations [6]. Recent studies have shown that date-palm waste can reduce thermal conductivity by 49% in earth bricks [13], whilst others report that the addition of pine needles can lead to up to ~24% higher compressive strength compared to straw reinforcement [5], with measured strengths of ~3.2–3.3 MPa versus ~2.7 MPa for straw. Organic waste has been validated as a means of reinforcing adobe. The residues from the paper and pulp industry, for example, have yielded up to 190% gains in compressive strength and a 30% decrease in thermal conductivity [14]. Furthermore, hemp-shiv reinforcement has been studied to increase flexural strength by 39% [15]. Additionally, bunho and junco fibers attain 20% enhancement in thermal insulation properties [16], and the use of fonio straw has been found to reduce thermal conductivity by up to ~67% at 1 wt% [17]. Mechanical performance peaks at ~0.2–0.4 wt% and may decline at higher dosages, indicating that the optimum level balances insulation gains with strength. Comparative studies of several types of fibers have also shown that wheat straw offers a good compromise between mechanical properties and water resistance [18].

In addition to fiber reinforcement, mineral additives such as bentonite have proven beneficial in enhancing cohesion, water resistance, and plasticity of earth-based materials. These properties are encouraged by the fine-grained alumino-silicate content of bentonite [19]. There is also the promise of bio-stabilization strategies, which use natural additives. Cow dung, for example, provides a 40% increase in mechanical strength stemming from synergistic organic-mineral interactions [20]. Dynamic compaction methods have also been shown to increase the compressive strength by 79% in combination with proper clay content [21].

While these enhancement approaches show significant promise, limited research has systematically compared additive performance across different soil mineralogies or examined how compositional parameters such as silica-to-alumina ratios correlate with mechanical and thermal outcomes. Additionally, the integration of disaster waste materials into adobe construction represents an underexplored opportunity for circular economy applications.

Dredged sediments and similar materials reused in construction have attracted significant international interest, thereby setting a precedent in other similar projects [22]. Adobe bricks have also been successfully integrated with construction waste materials; recycled powder demonstrates significant performance improvements and contributes to

the circular economy [23]. Various industrial waste materials such as ash and limestone sludge have also been effectively incorporated in the composition of adobe bricks as a means of sustainable waste-management [24].

In September 2024, Chiang Rai province was hit by extreme flooding that left sediments over 2 m high in the areas it affected, especially the Mae Sai district (Figure 1). These flood-derived sediments represent a major disposal problem as they are of large volume and can lead to unintended consequences if not properly disposed of. This paper thus investigates the possibility of recycling these deposits into a usable construction material by assessing their suitability to be made into adobe bricks. In order to create a control group, the soils used to make three commercially available adobe bricks were used as references, namely Nakhon Pathom (NPT), Sisaket (SSK), and Uttaradit (UTT), which represents established regional adobe production practices with the addition of natural fibers being common. More recent systematic research has established baseline ranges of mechanical properties of traditional adobe construction, with strong regional variations [25]. Rice husk was added to the Chiang Rai flood sediment (CRI) to enable comparability. Initial findings, nevertheless, showed that they were not strong enough when used alone. Therefore, bentonite was added as a second stabilizer to see whether rice husk, bentonite or the mixture of both could convert the sediment to a construction grade material.

Figure 1. Sediment accumulation in Mae Sai district, Chiang Rai, following the September 2024 flood.

Although the research of natural fibers and mineral additives has advanced, there are still a number of critical knowledge gaps that have not been filled. The majority of research has assessed additives individually and in a single-soil environment, and little focus has been made on the effects of various soil mineralogies on the performance of additives. Also, thermal performance is commonly underreported even though it is applicable in tropical climates [16], and no research has been performed linking adobe development with the reuse of sediment waste in circular construction plans. On the same note, experiments on non-traditional additives, like Bakelite, have demonstrated a decrease in compressive strength and a considerable enhancement in thermal insulation, which underscores thermal-mechanical trade-offs [26].

This research fills these knowledge gaps by using three main innovations: (1) systematic research on the relationships between soil mineralogy and additive effectiveness in various Thai soils, which form predictive frameworks, depending on the soil composition and plasticity properties; (2) dual-additive optimization between rice husk and sodium bentonite in gradual concentrations (5, 10, 15) to apply to the specific performance of flood sediments; and (3) comprehensive valorization of September 2024 Chiang Rai flood sediments as construction materials, investigating the potential for disaster waste transformation into functional building components.

2. Materials and Methods

2.1. Soil Sources and Additives

In this study, four types of soils are used, which include three commercial adobe soils of Nakhon Pathom (NPT), Sisaket (SSK), and Uttaradit (UTT), and a flood-derived sediment of Mae Sai District, Chiang Rai (CRI). The sample was taken after a flood on 27 September 2024, which left more than two meters of silt on the Sai River. Figure 2 demonstrates the geographic location of the sampling sites.

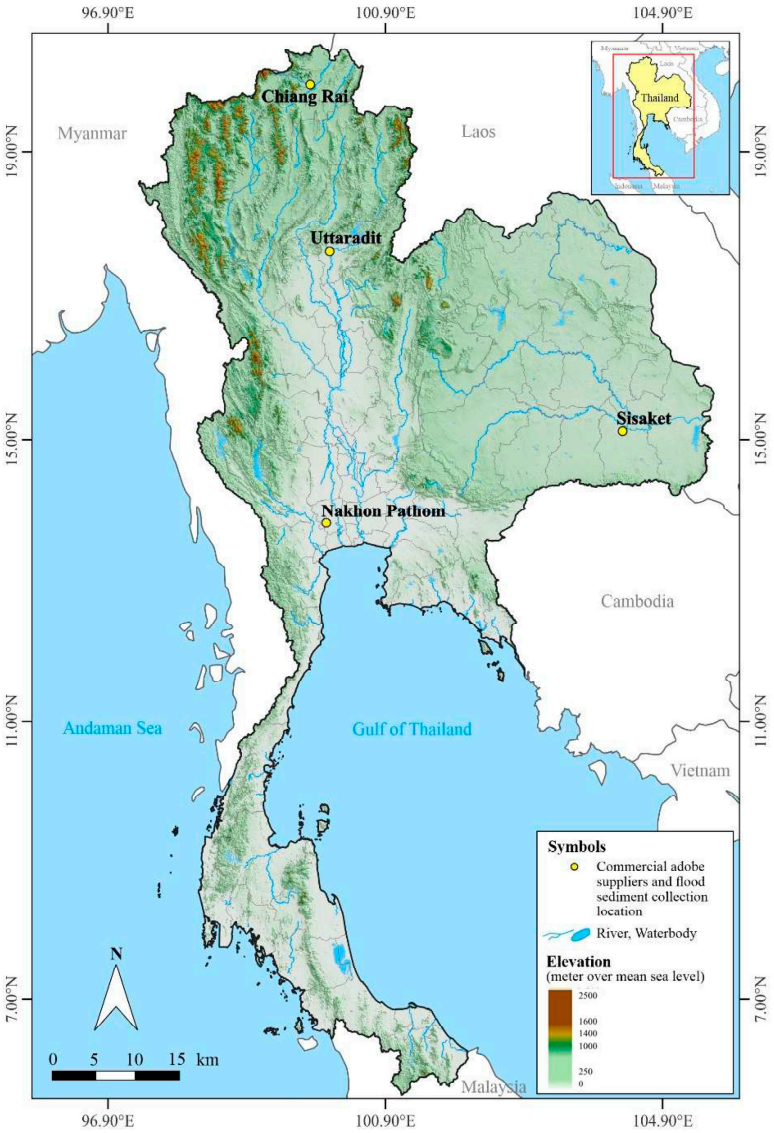

Figure 2. Geographic distribution of commercial adobe and flood sediment samples taken across Thailand.

Rice husk and sodium bentonite were chosen as the two additives to improve the engineering properties of the adobe bricks. Rice husk was obtained from local rice mills, while sodium bentonite was purchased from Thai Nippon Chemical Industry Co., Ltd. (Bangkok, Thailand) and was used exclusively in the CRI sediment mixtures. These additives were chosen based on the comprehensive research that showed the efficacy of fibers of agricultural waste [27,28] and mineral stabilizers [20] in earthen construction. Table 1 summarizes the chemical composition of the bentonite.

Figure 3 presents the particle size distributions of soils and additives. The particle size distribution of rice husk is coarse with 89.98% retained in the size above 4.75 mm offering fibrous strength to the adobe structure. Bentonite, in contrast, exhibits fine particle

properties, 97.29% of which pass through 0.075 mm, which is part of the cohesion and plasticity of the matrix. The soil gradations are intermediate with different distributions of the particles in the four types of soil. Table 2 shows the physical properties of the soil samples such as Atterberg limits and specific gravity.

Table 1. Chemical composition of sodium bentonite used in CRI mixtures.

Chemical Compound	Content (%)
Silicon dioxide (SiO_2)	46–60
Aluminum oxide (Al_2O_3)	14–17
Ferric oxide (Fe_2O_3)	6–8
Sodium oxide (Na_2O)	0.5–1.5
Magnesium oxide (MgO)	1.5–3.0
Calcium oxide (CaO)	1.0–2.5
Potassium oxide (K_2O)	0.1–1.0
Titanium dioxide (TiO_2)	0.2–1.5
Loss on ignition (LOI)	7–12

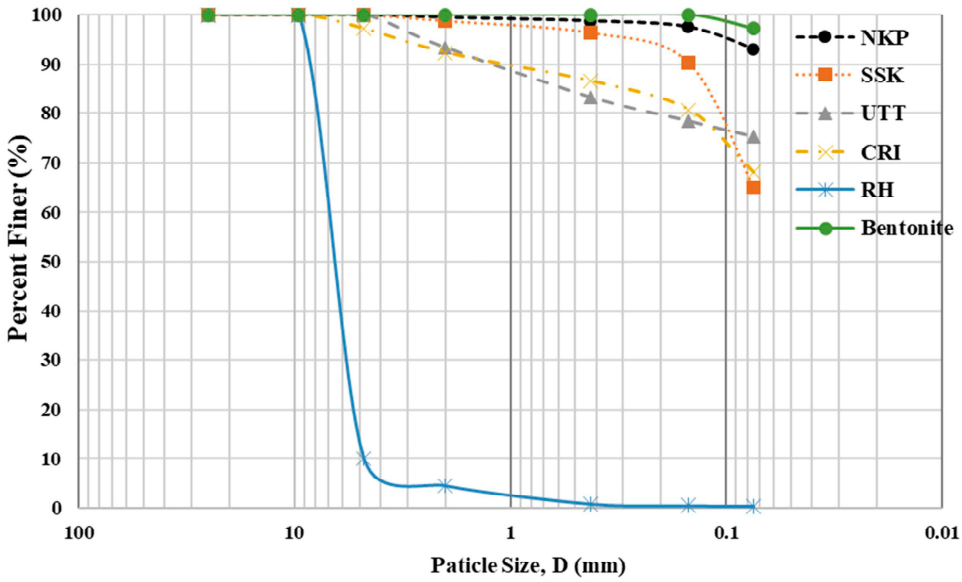

Figure 3. Particle size distribution curves of soils and additives showing distinct size ranges for mechanical reinforcement (rice husk) and matrix binding (bentonite).

Table 2. Physical properties of soil samples.

Soil	Liquid Limit (LL) (%)	Plastic Limit (PL) (%)	Plasticity Index (PI) (%)	Specific Gravity (Gs)
Nakhon Pathom (NPT)	42.70	21.33	21.37	2.65
Sisaket (SSK)	17.27	11.70	5.57	2.70
Uttaradit (UTT)	18.66	12.48	6.18	2.66
Chiang Rai (CRI)	31.55	NP	NP	2.66

The rice husk was obtained from local rice mills and sun-dried and sieved to a particle size smaller than 4 mm. Previous research has established optimal rice husk proportions for adobe applications in Southeast Asian contexts [11], providing guidance for our experimental design. Sodium bentonite, supplied by Thai Nippon Chemical Industry Co., Ltd., was used in powdered form to enhance plasticity and structural integrity. The bentonite contents (5%, 10%, and 15%) were selected based on preliminary trials showing that contents below 5% provided insufficient plasticity improvement while contents above 15% led to excessive material costs and potential workability issues during mixing and forming.

2.2. Soil Characterization

X-ray diffraction (XRD) was used to identify mineral phases in each soil (Figure 4). Quartz and kaolinite dominated the mineral profiles of the commercial adobe soils, while bentonite-containing mixes exhibited clear montmorillonite peaks. XRD patterns were collected using Cu–Kα radiation, scanned over 2θ = 10–80°. Phase identification was performed with reference to the Crystallography Open Database (COD). Semi-quantitative phase shares were estimated from relative peak intensities without Rietveld refinement, following established protocols for mineralogical characterization of earthen materials [29,30]. The results (Table 3) indicate quartz dominance in NPT (67%) and high alumina-bearing phases in UTT (40.4%). SSK showed an apparent dominance of TiO_2 reflections (55.5%), which is interpreted cautiously as a relative intensity artifact rather than absolute composition. This high TiO_2 content likely results from preferred orientation effects and high crystallinity of titanium phases relative to the clay matrix, rather than absolute weight percentage [31]. This interpretation is supported by SSK's moderate mechanical performance, which correlates with its 25.5% Al_2O_3 content rather than the apparent TiO_2 dominance.

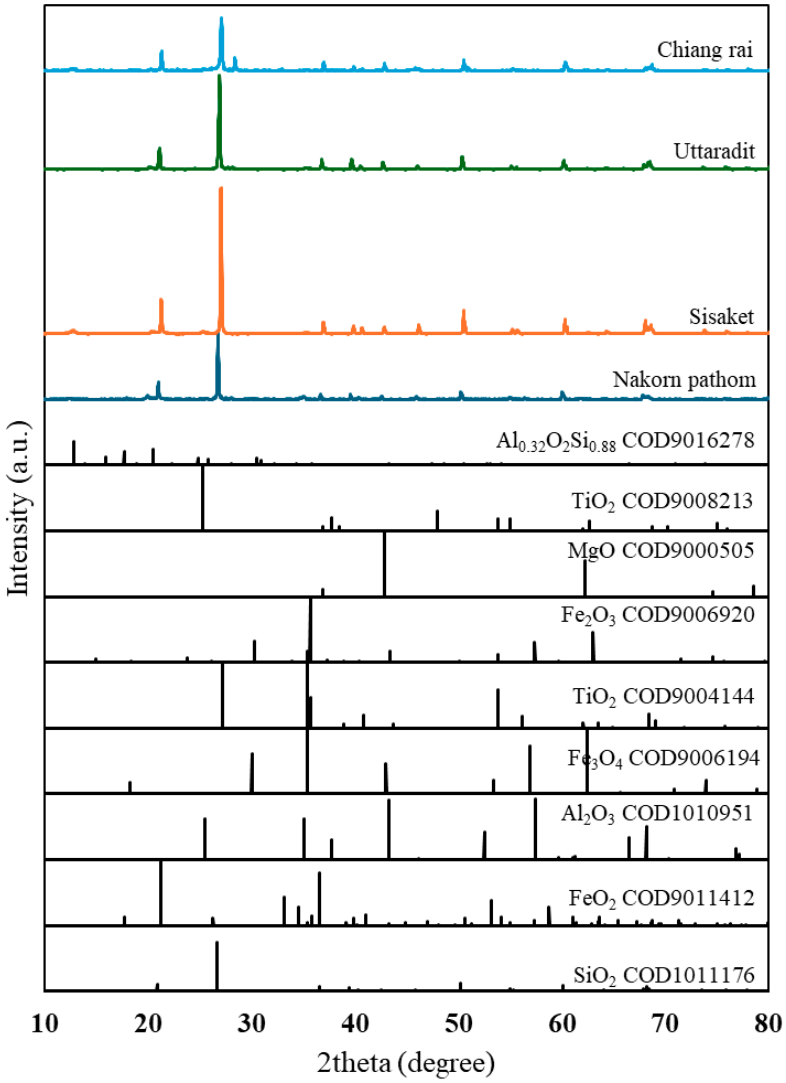

Figure 4. XRD patterns of adobe soils and CRI showing dominant mineral phases.

Scanning electron microscopy (SEM) was performed to assess particle morphology and bonding characteristics. CRI showed irregular particles with poor cohesion, while samples with bentonite showed improved microstructural integrity. SEM images are shown

in Figure 5. This microstructural analysis approach has been validated by multiple studies of fiber-reinforced earthen materials [12,32].

Table 3. Semi-quantitative phase composition of soils from XRD analysis.

Phase (COD Ref.)	Nakhon Pathom (NPT)	Sisaket (SSK)	Uttaradit (UTT)	Chiang Rai (CRI)
SiO_2—Quartz (1011176)	67.0	15.0	42.1	15.3
FeO_2 (9011412)	9.0	-	-	-
Al_2O_3—Corundum (1010951)	22.0	25.5	40.4	16.8
Fe_3O_4—Magnetite (9006194)	2.0	4.0	10.1	-
TiO_2—Rutile (9004144)	-	55.5	-	11.7
Fe_2O_3—Hematite (9006920)	-		7.4	-
MgO—Periclase (9000505)	-		-	41.8
TiO_2—Anatase (9008213)	-		-	7.0
$Al_{0.32}Si_{0.68}O_2$ (9016278)	-		-	7.4

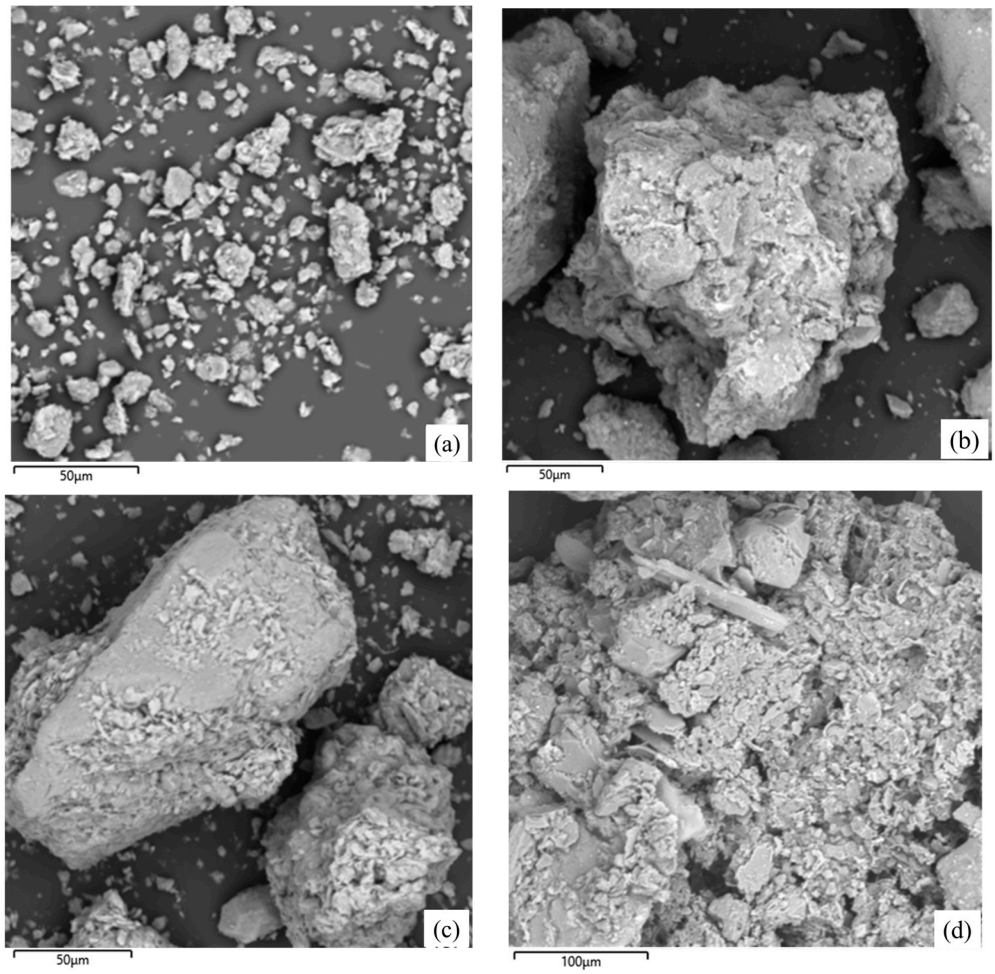

Figure 5. SEM images of adobe soil microstructures: (**a**) NPT, (**b**) SSK, (**c**) UTT, and (**d**) CRI.

Elemental composition was further confirmed using energy-dispersive X-ray spectroscopy (EDS), revealing notable differences across the four soil types. As shown in Table 4, oxygen and silicon were dominant in all samples, consistent with the presence of silicate minerals. The analytical framework follows established protocols for comprehensive soil characterization in earthen construction research [33].

Table 4. EDS elemental composition of adobe soils.

Soil	Representative Phase	O (wt%)	Si (wt%)	Al (wt%)	C (wt%)	Fe (wt%)	Other (wt%)
Nakhon Pathom (NPT)	Quartz-rich phase	32.8	42.4	2.1	15.9	1.0	K:0.4
Sisaket (SSK)	Lateritic clay phase	45.8	15.3	7.8	23.3	5.7	Ti:1.5, K:0.7
Uttaradit (UTT)	Mixed silicate phase	47.6	29.7	9.9	7.3	2.5	K:1.6, Na:0.9
Chiang Rai (CRI)	Detrital sediment phase	45.8	25.3	12.9	7.4	5.1	K:2.1, Ti:0.3

2.3. Adobe Brick Preparation

A total of twelve adobe brick formulations were prepared to investigate the effects of natural and mineral additives on different soil types. Soils from Nakhon Pathom (NPT), Sisaket (SSK), and Uttaradit (UTT) were each used to produce two formulations: raw soil only, and soil mixed with rice husk at approximately 3.45% by weight. For the sediment collected from Chiang Rai (CRI), six formulations were developed: CRI only, CRI with rice husk, CRI with 5% bentonite, and three combinations of CRI with rice husk and bentonite at 5%, 10%, and 15% by weight. The complete list of formulations is summarized in Table 5.

Table 5. Adobe brick formulations used in this study.

Code	Soil Type	Rice Husk (wt%)	Bentonite (wt%)
NPT	NPT	0	0
NPT + RH	NPT	3.45	0
SSK	SSK	0	0
SSK + RH	SSK	3.45	0
UTT	UTT	0	0
UTT + RH	UTT	3.45	0
CRI	CRI	0	0
CRI + RH	CRI	3.45	0
CRI + B5	CRI	0	5
CRI + RH + B5	CRI	3.45	5
CRI + RH + B10	CRI	3.45	10
CRI + RH + B15	CRI	3.45	15

The rice husk was collected in the local rice mills and dried under the sun and sieved to a size less than 4 mm. Past studies have set ideal proportions of rice husks to be used in adobe construction in Southeast Asian conditions [11], which will guide our experimental design. Thai Nippon Chemical Industry Co., Ltd. provided sodium bentonite in the form of powder to add plasticity and structural integrity. The water content was modified to each type of soil to give the appropriate workability and then the mixtures were left to soak over a period of 24 h to allow even distribution of moisture in the soil matrix. The moisture contents in the process of adobe bricks preparation differed greatly among the formulations: NPT + RH (38.29%), SSK + RH (22.56%), UTT + RH (17.26%), CRI + RH (49.93%), CRI + B5 (46.73%), CRI + RH + B5 (53.21%), CRI + RH + B10 (55.87%), and CRI + RH + B10 (57.81%). These values indicate the various water absorption properties of soil types and combinations of additives. The wet material was pressed into molds whose end brick size was 40 × 20 × 10 cm (Figure 6). The bricks were demolded and then subjected to shade and sun-dried in a period of two weeks to replicate the conditions of curing in the field. This is a preparation methodology that uses the standard procedures that have been tested in numerous natural fiber reinforcement studies [34,35].

Figure 6. Adobe specimen preparation process.

2.4. Mechanical and Thermal Testing

In order to measure the performance of adobe bricks, mechanical and thermal tests were performed in accordance with standardized procedures. The test matrix encompassed all the twelve adobe formulations, six of which were of commercial soils (NPT, SSK, UTT) and six of which were of CRI with different additive combinations.

A universal testing machine was used to test compressive strength of full-size adobe bricks with dimensions of 40 × 20 × 10 cm. The load was exerted on the 40 × 20 cm face in a vertical direction with a constant rate of displacement of 1.0 mm/min, in the general procedure of ASTM C67 of masonry units. Each formulation was tested on five specimens, and the results were deemed satisfactory when the coefficient of variation (COV) was not greater than 15%, which is also within variability ranges used in standardized adobe characterization research [25,36]. Figure 7 illustrates the test setup.

Figure 7. Compressive strength test setup for full-size adobe bricks under vertical loading.

Flexural strength was tested using full-size adobe bricks, positioned horizontally on two steel supports with a 30 cm span. A vertical load was applied at the midpoint through a rounded steel head to induce three-point bending. Although the setup was adapted from ASTM C78, the original dimensions of the bricks were maintained to represent real-world use cases. Five specimens per formulation were tested. Crack development and failure modes were observed and recorded during loading, following protocols established in recent natural fiber reinforcement research [26,27]. The test configuration and typical failure are shown in Figure 8a,b.

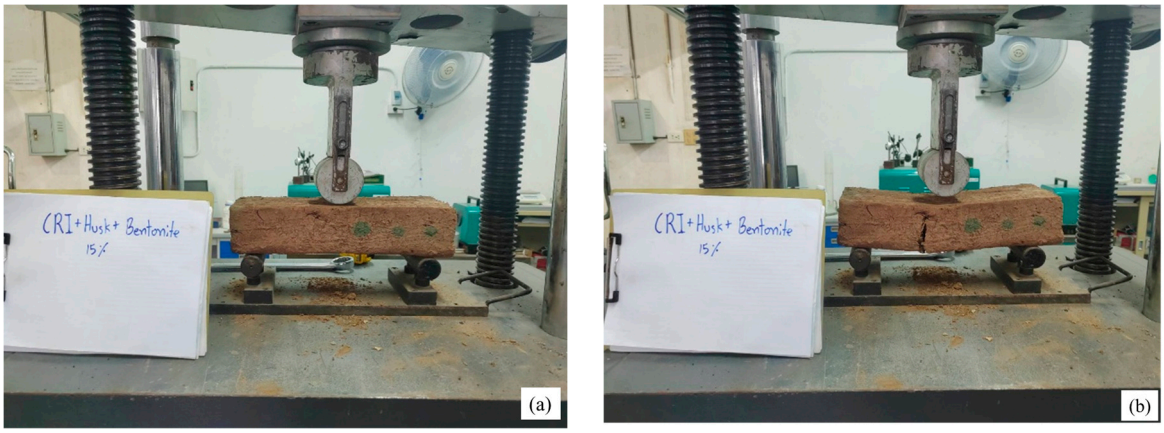

Figure 8. (**a**) Flexural strength test setup using full-size adobe brick under midspan loading. (**b**) Post-failure condition showing crack development and failure pattern.

Thermal conductivity was evaluated using a THERMTEST TLS-100 portable thermal analyzer (Thermtest, Hanwell, New Brunswick, Canada) applying the transient hot-wire method. Measurements were conducted on full-size adobe bricks after two weeks of sun-drying under controlled environmental conditions (temperature: 25 °C, relative humidity: 65 ± 10%). For each brick, five different surface locations were tested to account for heterogeneity across the material. The reported value per formulation represents the average of five bricks. This method follows the principles of ASTM C1113, adapted for low-conductivity porous materials, and is consistent with approaches used in recent thermal characterization studies of earthen materials [14,16]. The test procedure is shown in Figure 9.

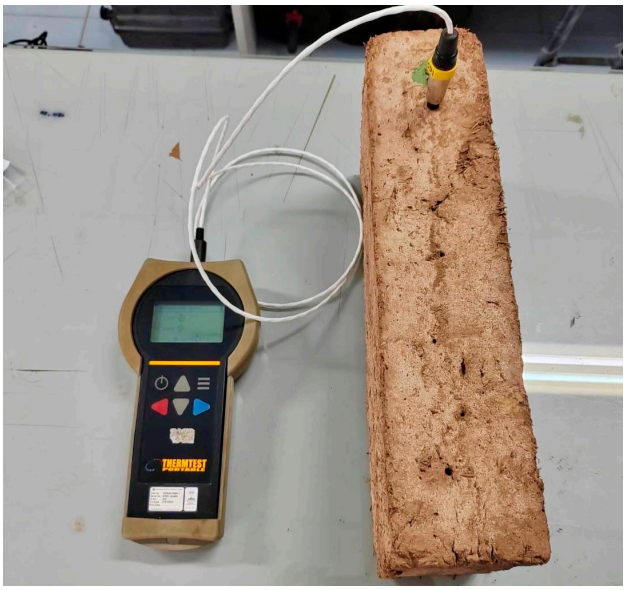

Figure 9. Thermal conductivity measurement using a THERMTEST analyzer with five test locations per full-size adobe brick.

3. Results

A total of twelve adobe formulations were developed to evaluate the influence of soil origin and additive combination on the mechanical and thermal performance of adobe bricks. The results are structured in three phases that reflect the material development pathway: initial evaluation of regional soil performance and reinforcement using rice husk

and optimization of flood-sediment adobe bricks with bentonite. Each stage includes detailed assessments of compressive strength, flexural strength, and thermal conductivity.

3.1. Baseline Performance of Regional Soils

Adobe performance varied across the four soil types, with distinct mechanical and thermal characteristics observed for each formulation (Figure 10). Uttaradit soil achieved the highest mechanical properties among all tested materials, with compressive strength of 1.71 ± 0.07 MPa and flexural strength of 0.35 ± 0.04 MPa. However, this superior mechanical performance corresponded with the highest thermal conductivity of 0.428 ± 0.006 W/m·K.

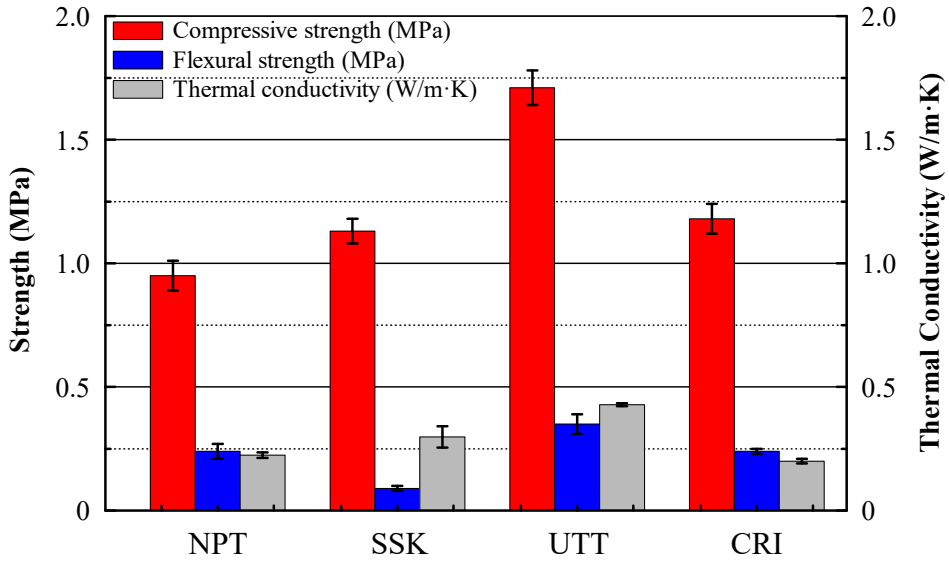

Figure 10. Baseline compressive strength, flexural strength, and thermal conductivity of adobe bricks made from untreated regional soils. Error bars represent standard deviation (SD) from five replicate specimens per formulation.

Chiang Rai flood sediment demonstrated moderate compressive strength (1.18 ± 0.06 MPa) and flexural strength of (0.24 ± 0.01 MPa) among all formulations. Notably, this material exhibited the lowest thermal conductivity (0.200 ± 0.009 W/m·K), indicating superior thermal insulation properties.

Nakhon Pathom and Sisaket soils showed compressive strengths of 0.95 ± 0.06 and 1.13 ± 0.05 MPa, respectively, with contrasting flexural behaviors: NPT achieved 0.24 ± 0.03 MPa while SSK reached 0.09 ± 0.01 MPa. Thermal conductivities were 0.224 ± 0.011 W/m·K for NPT and 0.298 ± 0.043 W/m·K for SSK.

The results reveal an inverse relationship between mechanical strength and thermal insulation performance: UTT provided optimal mechanical properties but limited thermal benefits, while CRI offered superior insulation with moderate structural capacity. NPT and SSK exhibited intermediate performance across both mechanical and thermal metrics, establishing distinct baseline characteristics for subsequent additive optimization studies.

3.2. Effects of Rice Husk Reinforcement

Rice husk incorporation produced systematic mechanical and thermal property modifications across all soil matrices, with enhancement magnitude correlating with mineralogical composition and baseline matrix characteristics (Figure 11).

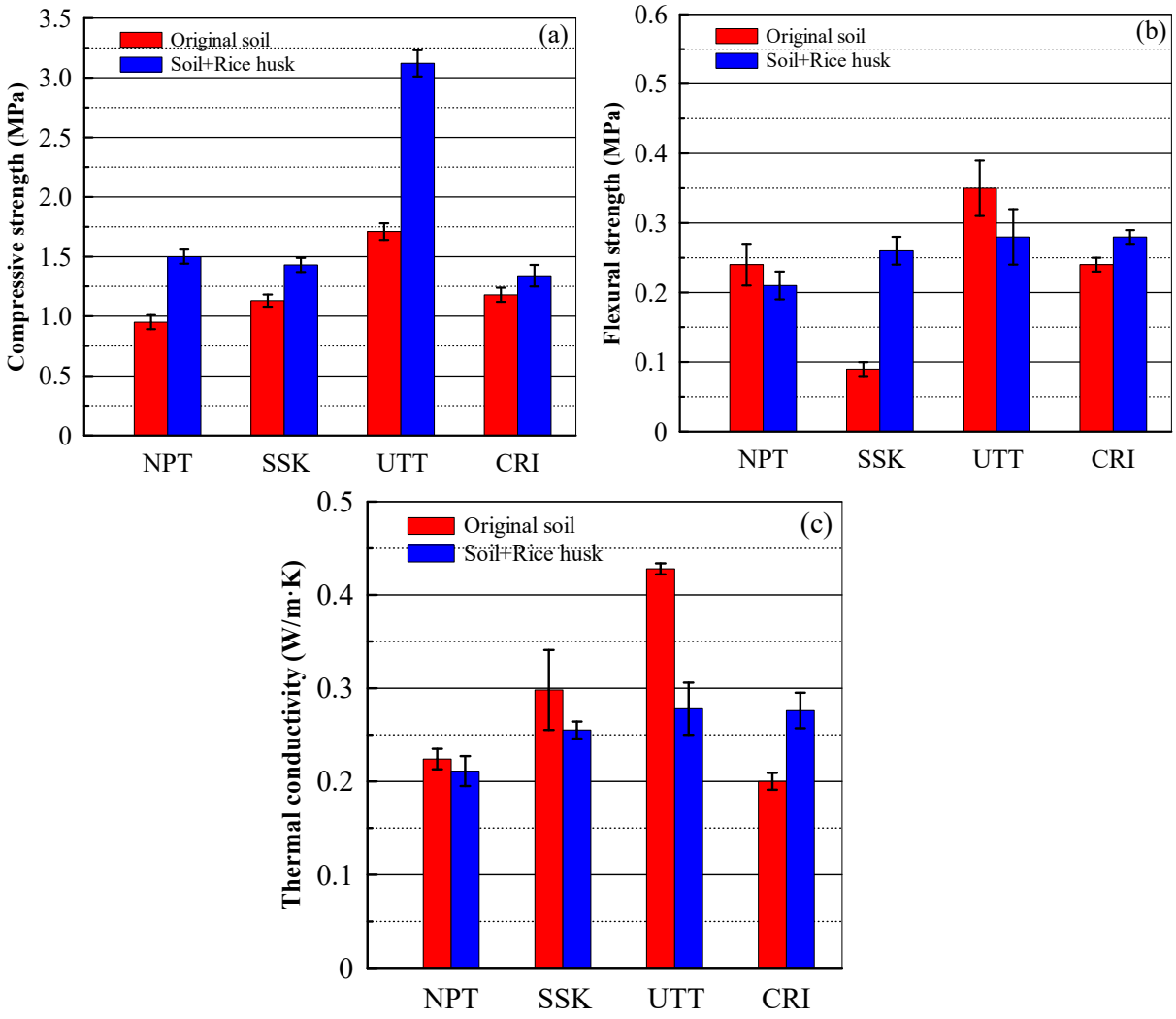

Figure 11. Effects of rice husk addition on adobe performance: (**a**) Compressive strength, (**b**) Flexural strength, and (**c**) Thermal conductivity across different soil types. Error bars represent standard deviation (SD) from five replicate specimens per formulation.

The compressive strength increased significantly across the soil types. The highest increase was observed in UTT, where 1.71 ± 0.07 MPa improved to 3.12 ± 0.11 MPa (82.5% increased). This was succeeded by NPT (57.9% increase to 1.50 ± 0.06 MPa), SSK (26.5% increase to 1.43 ± 0.06 MPa), and CRI (13.6% increase to 1.34 ± 0.09 MPa). The silica to alumina ratio can be used to rationalize the observed ranking, with UTT, which has a balanced composition (42.1% SiO_2 and 40.4% Al_2O_3), exhibiting optimal performance, and CRI, which has a more heterogeneous composition (15.3% SiO_2, 16.8% Al_2O_3), having limited enhancement efficacy.

The responses of flexural strength showed opposite trends. CRI experienced a significant positive change, with a 16.7% increase from 0.24 ± 0.01 to 0.28 ± 0.01 MPa, whilst the other soils exhibited decreases of between 4.5% in NPT and 34.9% in UTT, suggesting that the reinforcement behaviors were different in the various matrices.

All formulations showed an improvement in thermal conductivity with the following ranking of performance: NPT + RH (0.211 ± 0.016 W/m·K) < SSK + RH (0.255 ± 0.009 W/m·K) < CRI + RH (0.276 ± 0.019 W/m·K) < UTT + RH (0.278 ± 0.028 W/m·K). This shows that rice husk is a good renewable insulation additive. The trade-offs between density and porosity are reflected in the inverse correlation between mechanical strength and thermal insulation capacity, with high compressive performance and low insulation capacity.

Measurement variability varies across formulations. UTT + RH produced very similar results (relative coefficient of variation, CV = 3.56%), but CRI + RH was more variable (CV = 6.65%), as flood sediment deposits are heterogeneous. NPT + RH and SSK + RH exhibited intermediate variability, with CVs of 4.01% and 4.18%, respectively. These findings support the idea that mineralogical composition is the major factor that determines the effectiveness of reinforcement of rice husk, but the exact mechanisms that underlie soil-specific responses are not yet well understood without the in-depth micro-structural analysis.

3.3. Optimization of Flood Sediment with Bentonite

Complex material interactions and trade-offs in performance were evident in the systematic addition of bentonite to CRI flood sediment (Figure 12). The results of individual additives were opposite: the addition of rice husk (CRI+RH) resulted in an optimal compressive strength of 1.34 ± 0.09 MPa along with a thermal conductivity of 0.276 ± 0.019 W/m·K, and the addition of bentonite (CRI + B5) enhanced flexural strength to 0.40 ± 0.04 MPa, but decreased compressive strength to 0.85 ± 0.07 MPa and increased thermal conductivity to 0.404 ± 0.010 W/m·K. Dual-additive systems allowed balancing between the mechanical and thermal spectrum: CRI + RH + B5 had intermediate properties (0.82 ± 0.07 MPa compressive, 0.26 ± 0.01 MPa flexural, 0.263 ± 0.008 W/m·K thermal conductivity); CRI + RH + B10 had balanced properties (0.99 ± 0.02 MPa compressive, 0.23 ± 0.01 MPa flexural, 0.232 ± 0.013 W/m·K).

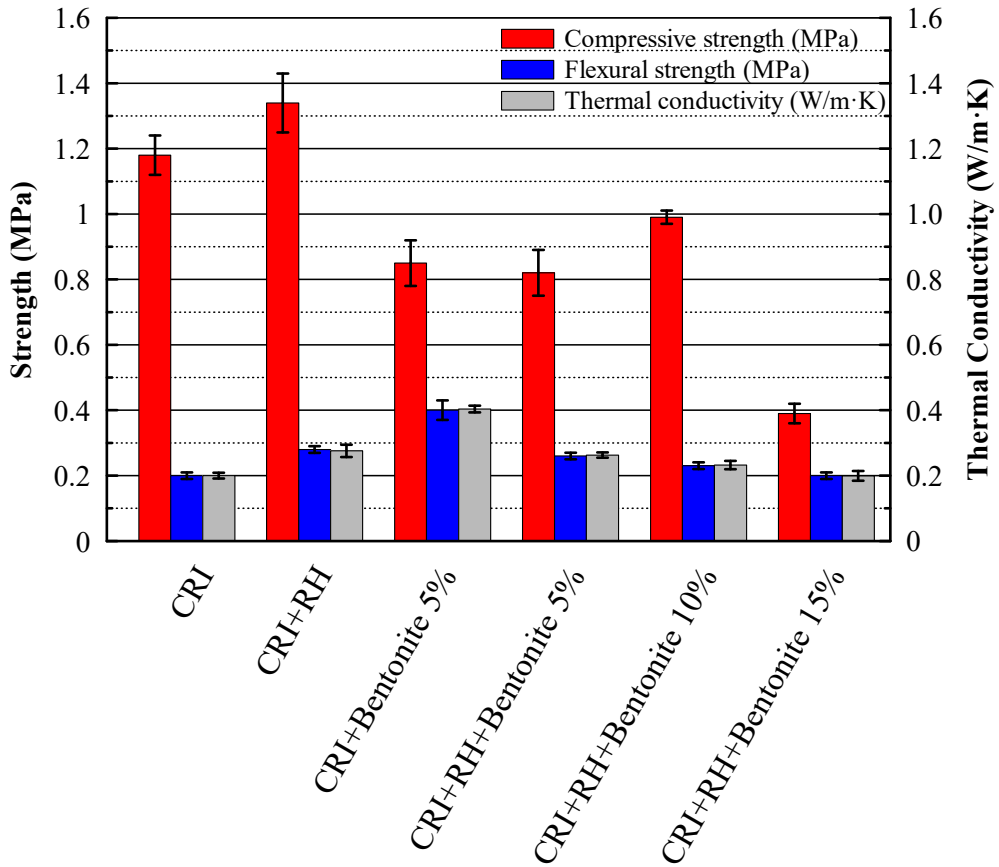

Figure 12. Performance characteristics of CRI adobe formulations with rice husk and varying bentonite content, demonstrating trade-offs between mechanical and thermal properties. Error bars represent standard deviation (SD) from five replicate specimens per formulation.

These data support systematic trade-offs which allow application-specific optimization: compressive strength is maximized by rice husk addition, moderate concentrations

of bentonite (5–10%) balance mechanical and thermal properties, and high concentrations of bentonite (15%) maximize thermal insulation at the expense of structural capacity. In this way, formulation strategies may be customized: maximum compressive strength with addition of sole rice husk, balanced properties with moderate addition of bentonite, or increased thermal properties with high addition of bentonite.

3.4. Microstructural Analysis

Optical microscopy with polarized light (OM-LIBs) was performed on selected formulations to understand the underlying mechanisms governing the observed mechanical and thermal performance variations. CRI + RH and CRI + RH + B10 were chosen for detailed microstructural examination as they represent contrasting optimization strategies: CRI + RH maximizes compressive strength (1.34 ± 0.09 MPa) while CRI + RH + B10 prioritizes thermal insulation (0.199 ± 0.015 W/m·K) with significantly reduced mechanical performance (0.39 ± 0.03 MPa).

CRI + RH formulations revealed rice husk fibers distributed heterogeneously throughout the flood sediment matrix with highly variable interfacial bonding characteristics (Figure 13a,b). The rice husk particles, ranging from 0.15 to 4.0 mm in length, formed a three-dimensional reinforcing network within the soil matrix. However, substantial void spaces were observed between matrix particles, and fiber-matrix adhesion varied significantly across the sample. Poor interfacial bonding in several regions correlates directly with the modest 13.6% compressive strength improvement compared to other soil types, while the abundant air voids explain the moderate thermal conductivity reduction to 0.276 ± 0.019 W/m·K.

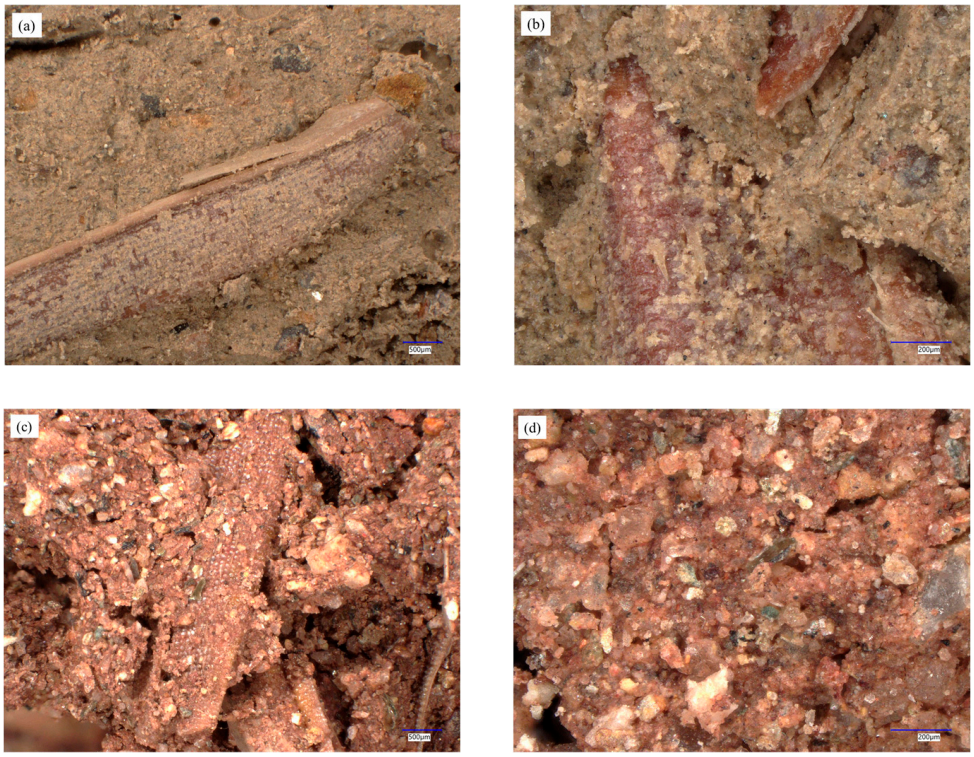

Figure 13. OM-LIBs images: (**a**) CRI + RH showing heterogeneous fiber distribution at 50× magnification, (**b**) CRI + RH detailed view at 200× magnification, (**c**) CRI + RH + B10 with dense bentonite-enhanced matrix at 50x magnification, and (**d**) CRI + RH + B10 detailed microstructure at 200× magnification.

In contrast, CRI + RH + B10 formulations exhibited fundamentally altered microstructural characteristics due to bentonite's binding and void-filling effects (Figure 13c,d). The

fine bentonite particles (97.29% passing 0.075 mm) effectively filled interparticle voids and created a significantly more continuous, dense matrix structure. This enhanced matrix continuity eliminated most air voids and improved particle packing efficiency, resulting in superior thermal insulation properties (0.199 ± 0.015 W/m·K). However, the increased density and reduced porosity contributed to matrix brittleness, explaining the substantial reduction in compressive strength to 0.39 ± 0.03 MPa.

The microstructural analysis reveals that rice husk provides mechanical reinforcement through fiber bridging in the heterogeneous CRI matrix, while bentonite addition fundamentally transforms the composite from a fiber-reinforced system to a dense, thermally optimized material. This microstructural understanding validates the observed trade-offs between mechanical and thermal performance in the dual-additive systems.

3.5. Rice Husk Reinforcement Mechanisms

The systematic change in rice husk performance in various soil matrices can be explained by a certain physicochemical interaction between the silica-rich rice husk (87.3% SiO_2) and the different soil mineral compositions. The reinforcement mechanisms act based on the chemical compatibility and physical interlocking effects.

UTT soil showed the best incorporation of rice husk because of the balanced ratio of SiO_2/Al_2O_3 (42.1%:40.4%), which gives the best silica-silica bonding and still has enough alumina phases to hold the matrix together. This chemical compatibility coupled with good load transfer mechanisms led to the maximum increase in compressive strength (82.5% improvement to 3.12 ± 0.11 MPa).

NPT soil, though rich in silica (67.0% SiO_2), was moderately enhanced (57.9% to 1.50 ± 0.06 MPa) because of the low alumina phases (22.0% Al_2O_3) to bind the matrix. SSK demonstrated a moderate performance (26.5% to 1.43 ± 0.06 MPa) that was associated with moderate alumina content (25.5% Al_2O_3), which validated the significance of balanced mineralogy in terms of the optimum fiber-matrix interaction.

CRI flood sediment is a special situation in which heterogeneous composition (15.3% SiO_2, 16.8% Al_2O_3) results in changing local bonding conditions. Although this reduces compressive enhancement (13.6% to 1.34 ± 0.09 MPa), it is the only matrix that enhances flexural strength (40% increase to 0.28 ± 0.01 MPa) by distributed fiber network effects. This mechanism is supported by the microstructural evidence in the form of three-dimensional fiber distribution that increases the resistance of cracks to bending loads.

The enhancement in thermal conductivity of all rice husk formulations (0.211–0.278 W/m·K range) is due to the induction of organic porosity and the low thermal conductivity of rice husk fibers (approximately 0.05–0.08 W/m·K) which forms effective insulation channels irrespective of the type of soil matrix.

4. Discussion

This section interprets the results presented earlier, shedding light on the material behavior, additive interactions, and underlying mechanisms that govern the performance of the studied adobe formulations. Three core findings emerge: the influence of soil mineral composition on baseline properties, the role of rice husk in enhancing mechanical and thermal properties, and the viability of bentonite for stabilizing flood-derived sediment. These insights contribute to a broader understanding of optimized material design for sustainable earthen construction.

4.1. Influence of Mineral Composition on Adobe Behavior

It was found that the mineralogical diversity of the soils under study had a strong impact on the adobe performance characteristics as it was shown in Table 6 and confirmed by

XRD analysis (Figure 4; Table 3). The correlation between the soil structure and performance shows some particular behaviors related to the prevalent mineral phases.

Table 6. Baseline mechanical properties comparison with soil mineralogy effects.

Soil Type	SiO_2 Content (%)	Compressive Strength (MPa)	Flexural Strength (MPa)	Thermal Conductivity (W/m·K)	Dominant Minerals
NPT	67.0	0.95 ± 0.06	0.24 ± 0.03	0.224 ± 0.011	Quartz-rich
SSK	15.0	1.13 ± 0.05	0.09 ± 0.01	0.298 ± 0.043	TiO_2, Fe oxides
UTT	42.1	1.71 ± 0.07	0.35 ± 0.04	0.428 ± 0.006	Balanced silica-alumina
CRI	15.3	1.18 ± 0.06	0.24 ± 0.01	0.200 ± 0.009	Detrital sediment
Silveira et al. [3]	-	0.66–2.15	0.19	-	Traditional mix [1]
Parisi et al. [4]	-	1.08	0.56	-	Clayey/silty sand [2]
Polidori et al. [29]	High $CaCO_3$	0.74–4.80	-	0.670	Chalky earth [3]

Note: [1] Traditional mix composed of coarse sand, argillaceous earth, and lime as reported by authors; [2] Clayey/silty sand (26.9% clay/silt, 70.1% sand, 3% gravel) with 0.64% straw fibers by weight; [3] Chalky earth with $CaCO_3$ content ranging from 0% to 84.9%; range reflects variation across 7 different soil compositions showing inverse relationship between carbonate content and compressive strength.

The Uttaradit soil, which had a balanced composition of silica-alumina (42.1% SiO_2, 40.4% Al_2O_3), had the best mechanical performance of all the soils tested with compressive strength of 1.71 ± 0.07 MPa and flexural strength of 0.35 ± 0.04 MPa. Nevertheless, the high thermal conductivity (0.428 ± 0.006 W/m·K) that comes with the high strength of UTT meant that the material had low insulation ability.

Although it is heterogeneous (15.3% SiO_2, 16.8% Al_2O_3), Chiang Rai flood sediment exhibited significant compressive strength (1.18 ± 0.06 MPa) and the highest insulation performance with the lowest thermal conductivity (0.200 ± 0.009 W/m·K). The correlation between the depositional source of the material and thermal performance needs further microstructural studies to be able to establish causative processes.

The soil of Nakhon Pathom with high silica content (67.0% SiO_2), had moderate mechanical (0.95 ± 0.06 MPa compressive, 0.24 ± 0.03 MPa flexural) and thermal (0.224 ± 0.011 W/m·K) behavior. These findings are in line with the findings in the Champagne region, which indicated that the quartz-dominated soils exhibit different yet moderate performance properties, which underscores the effects of mineralogical dominance on adobe performance [29].

Sisaket soil had similar compressive strength (1.13 ± 0.05 MPa) and intermediate flexural resistance (0.09 ± 0.01 MPa) and intermediate thermal conductivity (0.298 ± 0.043 W/m·K). The reported TiO_2 content of SSK (55.5%) is deemed to be an artifact of relative peak dominance and was not used in the interpretation of the properties (see Section 2.2). The intermediate flexural performance is associated with the small amount of alumina-bearing phases. This finding is consistent with the results that mineral composition influences mechanical behavior in earthen materials [33].

These findings define clear performance characteristics of the tested materials: UTT was found to have the best mechanical properties with balanced mineralogy, CRI was found to have the best thermal insulation with heterogeneous composition, and NPT and SSK were found to have intermediate properties. The overall inverse correlation of mechanical strength and thermal insulation of all soils in this study indicates material trade-offs, which should be considered in application-specific optimization strategies.

4.2. Mechanism of Rice Husk Reinforcement

Rice husk addition significantly enhanced adobe performance across all soil types, with the magnitude of improvement correlating with soil mineralogy and baseline material

characteristics (Table 7). The reinforcement effectiveness varied systematically among different soil matrices, as observed in this study, with underlying mechanisms revealed through microstructural analysis.

Table 7. Comparative performance of rice husk reinforced adobe against construction standards and natural fiber research.

Study/ Standard	Material/ Fiber Type	Content	Compressive Strength (MPa)	Flexural Strength (MPa)	Thermal Conductivity (W/m·K)
Current study					
NPT + RH	Rice husk	3.45%	1.50 ± 0.06	0.21 ± 0.02	0.211 ± 0.016
SSK + RH	Rice husk	3.45%	1.43 ± 0.06	0.26 ± 0.02	0.255 ± 0.009
UTT + RH	Rice husk	3.45%	3.12 ± 0.11	0.28 ± 0.04	0.278 ± 0.028
CRI + RH	Rice husk	3.45%	1.34 ± 0.09	0.28 ± 0.01	0.276 ± 0.019
International building standards					
IBC 2021 Section 2109	Unsterilized adobe	-	≥2.07	≥0.35	-
New Mexico Code 14.7.4	Adobe blocks	-	≥2.07	≥0.35	-
Los Angeles Code	Adobe masonry	-	≥1.55	-	-
Previous research					
Silveira et al. [3]	Traditional adobe	-	0.66–2.15	0.19	-
Parisi et al. [4]	Clayey/silty sand	0.64% straw	1.08	0.56	-
Polidori et al. [29]	Chalky earth	Variable $CaCO_3$	0.74–4.80	-	0.670
Natural fiber reinforcement					
Kasie and Mogne [6]	Sisal fiber	0.90%	13.44	0.10	-
Sriwattanaprayoon [11]	Rice husk	6.35–11.05%	1.32–2.13	0.32–0.73	
Eslami et al. [12]	Palm fiber	0.25%	4.88	0.22	-
Khoudja et al. [13]	Date palm waste	10.00%	0.55	0.29	0.342
Rocco et al. [16]	Bunho/junco fibers	3.00%	-	-	0.980
Millogo et al. [27]	Hibiscus cannabinus	0.40%	2.90	1.30	-

Uttaradit soil demonstrated the most substantial improvements with rice husk addition, achieving compressive strength increases of 82.5% (from 1.71 ± 0.07 to 3.12 ± 0.11 MPa) while experiencing flexural strength reduction of 20.0% (from 0.35 ± 0.04 to 0.28 ± 0.04 MPa). This performance profile indicates complex interactions between the fiber additive and UTT's balanced mineralogy (42.1% SiO_2, 40.4% Al_2O_3), though detailed interfacial analysis would be necessary to elucidate specific mechanisms.

Nakhon Pathom soil exhibited substantial improvements with rice husk incorporation, achieving compressive strength enhancement of 57.9% to 1.50 ± 0.06 MPa and flexural strength reduction of 12.5% to 0.21 ± 0.02 MPa. The quartz-dominated composition (67.0% SiO_2) correlates with this balanced enhancement pattern, though the relationship requires microstructural investigation to establish causative factors.

Sisaket soil showed moderate compressive strength improvements of 26.5% to 1.43 ± 0.06 MPa with flexural strength increases of 189% to 0.26 ± 0.02 MPa. Chiang Rai sediment demonstrated contrasting behavior with modest compressive gains of 13.6% to 1.34 ± 0.09 MPa but exceptional flexural enhancement of 16.7% to 0.28 ± 0.01 MPa. This unique flexural response, where both CRI and SSK improved while NPT and UTT decreased, reflects the different reinforcement mechanisms across soil matrices and suggests that heterogeneous compositions can enable alternative fiber-matrix interaction pathways.

The particle size analysis reveals that rice husk exhibits predominantly coarse particles, with 89.98% retained above 4.75 mm sieve size, providing fibrous reinforcement within the adobe matrix. The moisture content during casting varies significantly among formulations: CRI + RH (49.93%), NPT + RH (38.29%), SSK + RH (22.56%), and UTT + RH (17.26%), indicating different water absorption characteristics that may influence bonding behavior.

Microstructural analysis using optical microscopy with polarized light (OM-LIBs) reveals distinct characteristics between CRI + RH and CRI + RH + B10 systems. The CRI + RH samples show individual rice husk fibers appearing as elongated, light brown to tan colored tubular structures embedded within the darker brown soil matrix. The fibers display a hollow, cellular structure typical of plant cellulose with visible void spaces around the fiber-matrix interfaces. The matrix appears heterogeneous with variable particle sizes and colors, creating a loose, porous microstructure that explains both the modest compressive improvement (13.6%) and the unique flexural enhancement (16.7%) observed in CRI formulations.

In contrast, the CRI + RH + B10 samples exhibit a fundamentally different microstructure, characterized by a much denser, more uniform reddish-brown matrix. The fine bentonite particles appear to have filled the void spaces and created a more continuous matrix structure. The overall microstructure is significantly denser and more homogeneous compared to the CRI + RH system, with reduced porosity. Measurement analysis indicates that rice husk fibers in this system maintain lengths over 1200 μm, but they are more intimately bonded within the denser bentonite-enhanced matrix. This denser microstructure correlates with the superior thermal insulation properties (0.199 ± 0.015 W/m·K) but reduced mechanical performance (0.39 ± 0.03 MPa compressive) of the CRI + RH + B10 formulation.

The microstructural comparison reveals that rice husk has been shown to reinforce by physical fiber bridging in the loose CRI matrix, and addition of bentonite fundamentally changes the composite behavior by forming a dense, thermally optimized material by filling in the voids and densifying the matrix. The apparent disparity in porosity and matrix continuity between the two systems confirms the apparent trade-offs between mechanical strength and thermal performance.

The enhancement of thermal conductivity was observed in all rice husk formulations and the thermal conductivity varied between 0.211 ± 0.016 W/m·K (NPT+RH) to 0.278 ± 0.028 W/m·K (UTT+RH). The thermal improvement is negatively proportional to mechanical per-performance, which means that there are material trade-offs affecting application-specific optimization strategies. These thermal gains indicate that rice husk can be an effective renewable additive to enhance insulation and this is probably because it introduces air pores around the fibers as well as because the organic fiber material itself has low thermal conductivity.

4.3. Optimization of Flood Sediment Using Bentonite

Systematic optimization of CRI flood sediment with bentonite demonstrated viable pathways for converting disaster waste into functional building materials, as evidenced by the comprehensive performance evaluation shown in Table 8. The dual additive approach

addressed the inherent limitations of heterogeneous flood sediment while maintaining its superior thermal characteristics.

Table 8. CRI optimization compared with international standards and waste valorization approaches.

Material/ Standard	Additive Strategy	Density (kg/m^3)	Compressive Strength (MPa)	Flexural Strength (MPa)	Thermal Conductivity (W/m·K)
International building standards					
IBC 2021 Section 2109	Unsterilized adobe	-	≥2.07	≥0.35	-
New Mexico Code 14.7.4	Adobe blocks	-	≥2.07	≥0.35	-
Los Angeles Code	Adobe masonry	-	≥1.55	-	-
Current study					
CRI	-	1534	1.18 ± 0.06	0.24 ± 0.01	0.200 ± 0.009
CRI+RH	Single fiber	1320	1.34 ± 0.09	0.28 ± 0.01	0.276 ± 0.019
CRI + 5% Bentonite	Mineral stabilizer	1411	0.85 ± 0.07	0.40 ± 0.03	0.404 ± 0.010
CRI + RH + 5% Bentonite	Dual system	1203	0.82 ± 0.07	0.26 ± 0.01	0.263 ± 0.008
CRI + RH + 10% Bentonite	Dual system	1116	0.99 ± 0.02	0.23 ± 0.01	0.232 ± 0.013
CRI + RH + 15% Bentonite	Dual system	1076	0.39 ± 0.03	0.20 ± 0.01	0.199 ± 0.015
Waste valorization research					
Pachamama et al. [20]	Cow dung 10%	1790	0.90	0.45	-
Dormohamadi and Rahimnia [21]	Dynamic compaction	-	2.23–8.11	0.43–1.31	-
Zeng et al. [23]	Recycled powder	-	12.00–13.00	-	-
Călătan et al. [24]	Industrial waste	1650–1690	8.20	1.80	-
Hussain et al. [37]	Dredged sediment	1330–1523	0.34–2.93	-	-

Single additive systems revealed distinct enhancement mechanisms. Rice husk addition alone (CRI+RH) achieved the highest compressive strength of 1.34 ± 0.09 MPa, representing a 13.6% improvement over the untreated CRI baseline (1.18 ± 0.06 MPa). This enhancement also improved flexural performance from 0.24 ± 0.01 to 0.28 ± 0.01 MPa (16.7% increase). Conversely, bentonite addition alone (CRI + B5) demonstrated contrasting behavior with reduced compressive strength (0.85 ± 0.07 MPa) but improved flexural strength (0.40 ± 0.04 MPa) and increased thermal conductivity to 0.404 ± 0.010 W/m·K, indicating reduced insulation performance.

Dual additive systems enabled systematic property customization to suit specific application requirements. The CRI + RH + B5, CRI + RH + B10 and CRI + RH + B10 formulations demonstrated that increasing bentonite content alters material behavior in predictable patterns: CRI + RH + B5 achieved 0.82 ± 0.07 MPa compressive strength and 0.26 ± 0.01 MPa flexural strength with moderate thermal conductivity (0.263 ± 0.008 W/m·K); CRI + RH + B10 provided balanced properties with 0.99 ± 0.02 MPa compressive strength and 0.23 ± 0.01 MPa flexural strength while maintaining good thermal conductivity (0.232 ± 0.013 W/m·K). Higher bentonite content (CRI + RH + B10) resulted in reduced mechanical performance

(0.39 ± 0.03 MPa compressive, 0.20 ± 0.01 MPa flexural) but achieved superior thermal insulation (0.199 ± 0.015 W/m·K).

The microstructural examination shows the basic variations in composite behavior. Figure 13c,d indicate that CRI + RH + B10 formulations had significantly changed microstructural properties as a result of the binding and void-filling properties of bentonite. The small curved particles of bentonite (97.29% through 0.075 mm) were effective in filling interparticle voids and forming a much more continuous, dense matrix structure. This increased continuity of the matrix and removed the majority of air pores and increased the efficiency of particle packing leading to excellent thermal insulation. Nevertheless, the higher density and the lower porosity were the factors that enhanced the brittleness of the matrix, which is why the compressive strength had decreased significantly.

These findings define definite optimization directions: rice husk is the best material to maximize compressive properties, moderate levels of bentonite (5–10%) are the best to balance mechanical and thermal properties, and high levels of bentonite (15%) are the best to maximize thermal insulation at the cost of structural capacity. Although the effects of bentonite differ greatly across material systems [38], the observed systematic trade-offs in this work make it possible to design adobe structures using application-specific material. The results offer quantitative advice to the valorization of flood sediment in construction projects, but the practical application of the results must consider the economic factors, processing scalability, and long-term durability performance that were not studied in the present study.

4.4. Strategic Implications for Sustainable Construction

This research establishes a systematic framework for adobe optimization based on local soil mineralogy and available waste streams, supporting both circular economy principles and climate-responsive building strategies. The experimental findings demonstrate practical pathways for material optimization that align with regional resource availability.

The integration of rice husk, a readily available agricultural by-product in Thailand, with commercially available bentonite creates a circular material protocol consistent with waste valorization approaches documented in construction materials research [23,38]. The superior performance achieved with UTT-based formulations (3.12 ± 0.11 MPa compressive strength) and the successful enhancement of CRI flood sediment (thermal conductivity improved to 0.276 ± 0.019 W/m·K) demonstrate that additive effectiveness correlates with soil chemistry, though the specific mechanisms require further investigation.

The systematic enhancement of flood sediment demonstrates potential pathways for disaster waste utilization in construction applications. CRI formulations achieved compressive strengths up to 1.34 ± 0.09 MPa and flexural strengths up to 0.40 ± 0.04 MPa with bentonite addition, indicating suitability for non-structural applications such as interior partitions and thermal insulation systems. These performance levels provide alternatives for post-disaster reconstruction while addressing waste management challenges. While Thailand lacks formal standards for unburnt adobe bricks, preliminary quality guidelines suggest minimum compressive strength of 2.07 MPa. Among the tested formulations, UTT + RH (3.12 ± 0.11 MPa) significantly exceeds this benchmark, while most CRI-based formulations remain suitable for non-structural applications.

The integration of local waste streams with regional soil resources offers potential benefits through reduced material transportation requirements and waste valorization. Consistent thermal performance improvements across all rice husk formulations (0.211–0.278 W/m·K range) compared to baseline soil performance (0.200–0.428 W/m·K range) demonstrate enhanced insulation characteristics suitable for tropical building applications where thermal comfort is paramount.

This research contributes to broader waste-to-construction-material development, supported by parallel investigations of paper and pulp residues [14] and other organic waste applications in earthen construction. This approach aligns with Thailand's Bio-Circular-Green economic development framework through agricultural residue utilization, disaster waste reuse, and low-carbon construction alternatives. However, successful implementation requires addressing scaling considerations, economic feasibility analysis, and regulatory compliance that extend beyond the current laboratory-scale investigation.

Figure 14 demonstrates practical implementation of adobe construction techniques in Thailand, showing the feasibility of earthen building applications in real-world contexts.

Figure 14. Adobe construction example at Khon Kaen University, Thailand, demonstrating earthen building applications.

4.5. Sustainability Assessment and Implementation Implications

Adobe construction shows great environmental benefits with its significantly lower embodied carbon compared to traditional masonry material. Life-cycle analyses approximate embodied carbon of 0.00175–0.01250 kg CO_2eq/kg for adobe systems [39], compared to about 0.24 kg CO_2eq/kg of fired clay bricks and 0.23 kg CO_2eq/kg of concrete blocks [40]. The main cause of this order-of-magnitude difference is the removal of energy-intensive firing processes and the use of solar drying methodologies.

Environmental value goes beyond material production by using localized sourcing strategies. The locally sourced soil and agricultural residues are normally used in Adobe production, thus significantly lowering the transportation-related emissions [39]. Such a localized strategy is consistent with the principles of circular construction as it incorporates the waste streams regionally and reduces the impact of supply chains. Also, the thermal mass characteristics of adobe lead to less operational energy use, as it requires less mechanical cooling, which also provides environmental and occupant comfort advantages.

The environmental case is backed by economic analysis in terms of life-cycle cost benefits. The cost benefits are based on the fact that there is less material transportation, less maintenance needs, and no industrial processing [41]. Local material integration and simplified production techniques opens economic opportunities and minimize capital investment requirements.

This combination of environmental and economic considerations makes the use of adobe construction a feasible low-carbon alternative that promotes sustainable building practices due to its low environmental impact and higher economic accessibility. This research contributes to broader waste-to-construction-material development, supported by parallel investigations of paper and pulp residues [14] and other organic waste applications

in earthen construction. This approach aligns with Thailand's Bio-Circular-Green economic development framework through agricultural residue utilization, disaster waste reuse, and low-carbon construction alternatives.

5. Conclusions

This study systematically evaluated the mechanical and thermal characteristics of adobe bricks produced using four types of Thai soils, namely Nakhon Pathom (NPT), Sisaket (SSK), Uttaradit (UTT), and flood-derived sediment in Chiang Rai (CRI) with the addition of rice husk and sodium bentonite. The findings establish quantitative relationships between soil mineralogy and material performance while demonstrating viable pathways for disaster waste valorization through innovative dual-additive optimization.

The mineral composition of soil definitively influences adobe performance characteristics. Uttaradit soil with balanced SiO_2/Al_2O_3 ratios (42.1%:40.4%) achieved optimal mechanical properties (3.12 ± 0.11 MPa compressive strength with rice husk addition), while Chiang Rai flood sediment with heterogeneous composition (15.3% SiO_2, 16.8% Al_2O_3) demonstrated superior thermal insulation (0.200 ± 0.009 W/m·K). These findings provide predictive frameworks for material selection based on mineralogical characteristics.

Rice husk reinforcement systematically increased compressive strength in all soil matrices (13.6–82.5% improvement) and consistently increased thermal performance (0.211–0.278 W/m·K). The magnitude of the enhancement was directly proportional to the soil mineralogy, UTT recorded the highest absolute strength enhancement (82.5% to 3.12 ± 0.11 MPa), although the flexural strength declined by 34.9%. Microstructural examination showed that rice husk could reinforce mechanically by forming three-dimensional fiber networks and provide desirable porosity to act as thermal insulation.

Dual-additive strategies of flood sediment optimization allowed customization of materials according to application. CRI + RH gave the best compressive strength (1.34 ± 0.09 MPa), CRI + RH + B10 balanced (0.99 ± 0.02 MPa compressive, 0.232 ± 0.013 W/m·K thermal) and CRI + RH + B10 gave the best thermal insulation (0.199 ± 0.015 W/m·K) where non-structural applications are needed. This is a systematic trade-off that enables adobe bricks to be customized to suit construction requirements.

This study defines the material selection principles into practical use: UTT-based formulations are applicable to high-strength structural projects, NPT and SSK formulations are applicable in general construction projects, and CRI-based systems are applicable in thermal insulation and post-disaster reconstruction projects. Flood sediment valorization aligns with the Bio-Circular-Green economic development model of Thailand, which helps in sustainable building practices and the principles of the circular economy.

There are several limitations that should be taken into consideration to fully implement it. The ongoing experiment is on laboratory scale specimens of two-week curing time, which might not be a complete reflection of long-term durability in the field. The characteristics of weathering resistance, freeze–thaw cycling, and moisture absorption demand specific research to be thoroughly evaluated in terms of performance. The shift in the laboratory mixing to industrial production presents the issues of quality control, homogeneity maintenance, and economic optimization that need pilot-scale studies.

While the OM-LIBs analysis reveals fundamental mechanisms, quantitative image analysis and additional characterization techniques would strengthen the mechanistic understanding. This study does not include analysis of dimensional stability, creep behavior, or bond strength with mortar systems relevant for practical construction applications. Implementation requires consideration of technical standardization, quality control procedures, and compatibility with current building regulations. Comprehensive economic

analysis should consider quality control costs, skill development requirements, and regulatory compliance expenses.

These results advance adobe material science by establishing quantitative relationships between soil composition and performance while demonstrating practical pathways for disaster waste utilization. The low processing requirements and utilization of locally accessible raw materials make adoption feasible in resource-limited settings, contributing to waste management solutions and affordable housing development.

Author Contributions: Conceptualization, A.K. and S.E.-A.; methodology, A.K. and S.E.-A.; validation, S.E.-A. and R.A.; formal analysis, A.K. and N.C.; investigation, A.K.; resources, A.K. and S.E.-A.; data curation, S.E.-A. and N.C.; writing—original draft preparation, A.K. and S.E.-A.; writing—review and editing, A.K. and S.E.-A.; visualization, A.K., S.E.-A. and R.A.; supervision, S.E.-A. and R.A. All authors have read and agreed to the published version of the manuscript.

Funding: This research received no external funding.

Data Availability Statement: The original contributions presented in this study are included in the article. Further inquiries can be directed to the corresponding author.

Acknowledgments: The authors acknowledge Ten Consultant Company Limited for their assistance in conducting the thermal conductivity testing. Special thanks to Anirut Nitas from Underground Investigation Company Limited for sample preparation. The authors gratefully acknowledge additional technical support provided during the experimental phase of this research.

Conflicts of Interest: The authors declare no conflicts of interest.

References

1. Illampas, R.; Ioannou, I.; Charmpis, D.C. Adobe: An environmentally friendly construction material. *WIT Trans. Ecol. Environ.* **2009**, *120*, 245–256. [CrossRef]
2. Brito, M.R.; Marvila, M.T.; Linhares, J.A.T., Jr.; Azevedo, A.R.G. Evaluation of the properties of adobe blocks with clay and manure. *Buildings* **2023**, *13*, 657. [CrossRef]
3. Silveira, D.; Varum, H.; Costa, A.; Martins, T.; Pereira, H.; Almeida, J. Mechanical properties of adobe bricks in ancient constructions. *Constr. Build. Mater.* **2012**, *28*, 36–44. [CrossRef]
4. Parisi, F.; Asprone, D.; Fenu, L.; Prota, A. Experimental characterization of Italian composite adobe bricks reinforced with straw fibers. *Compos. Struct.* **2015**, *122*, 300–307. [CrossRef]
5. Jové-Sandoval, F.; Barbero-Barrera, M.M.; Flores Medina, N. Assessment of the mechanical performance of three varieties of pine needles as natural reinforcement of adobe. *Constr. Build. Mater.* **2018**, *187*, 205–213. [CrossRef]
6. Kasie, Y.M.; Mogne, A.Y. Improvement of mechanical properties of adobe brick reinforced with sisal fiber. *Discov. Mater.* **2025**, *5*, 69. [CrossRef]
7. Gomes, C.C.; Delucis, R.A.; Theisen, K.M. Valorization of piassava fiber by its incorporation in adobe bricks. *An. Acad. Bras. Ciênc.* **2024**, *96* (Suppl. S3), e20240210. [CrossRef] [PubMed]
8. Kumar, N.; Mehta, V.; Kumar, S.; Singh, J.P.; Kumar, R.; Sharma, S.; Dwivedi, S.P.; Kozak, D.; Lozanovic, J.; Abbas, M. An investigation of various properties of hybrid bricks using natural fibers and waste fiber-based materials. *J. Eng. Fibers Fabr.* **2024**, *19*, 15589250241240073. [CrossRef]
9. Olacia, E.; Pisello, A.L.; Chiodo, V.; Maisano, S.; Frazzica, A.; Cabeza, L.F. Sustainable adobe bricks with seagrass fibres: Mechanical and thermal properties characterization. *J. Nat. Fibers* **2020**, *17*, 1235–1247. [CrossRef]
10. Srisuwan, L.; Jarukumjorn, K.; Suppakarn, N. Physical Properties of Rice Husk Fiber/Natural Rubber Composites. *Adv. Mater. Res.* **2012**, *410*, 90–93. [CrossRef]
11. Sriwattanaprayoon, N. Engineering properties of adobe brick for earth structures. *IJERD—Int. J. Environ. Rural Dev.* **2014**, *5*, 41–46.
12. Eslami, A.; Mohammadi, H.; Mirabi Banadaki, H. Palm fiber as a natural reinforcement for improving the properties of traditional adobe bricks. *Constr. Build. Mater.* **2022**, *325*, 126808. [CrossRef]
13. Khoudja, D.; Taallah, B.; Izemmouren, O.; Aggoun, S.; Herihiri, O.; Guettala, A. Mechanical and thermophysical properties of raw earth bricks incorporating date palm waste. *Constr. Build. Mater.* **2021**, *270*, 121824. [CrossRef]
14. Muñoz, P.; Letelier, V.; Muñoz, L.; Bustamante, M.A. Adobe bricks reinforced with paper & pulp wastes improving thermal and mechanical properties. *Constr. Build. Mater.* **2020**, *254*, 119314. [CrossRef]

15. Hussain, M.; Levacher, D.; Saouti, L.; Leblanc, N.; Zmamou, H.; Djeran-Maigre, I.; Razakamanantsoa, A. Implementation on a preparation and controlled compaction procedure for waste-fiber-reinforced raw earth samples. *J. Compos. Sci.* **2022**, *6*, 3. [CrossRef]
16. Rocco, A.; Vicente, R.; Rodrigues, H.; Ferreira, V. Adobe blocks reinforced with vegetal fibres: Mechanical and thermal characterisation. *Buildings* **2024**, *14*, 2582. [CrossRef]
17. Ouedraogo, M.; Dao, K.; Millogo, Y.; Aubert, J.-E.; Messan, A.; Seynou, M.; Zerbo, L.; Gomina, M. Physical, thermal and mechanical properties of adobes stabilized with fonio (*Digitaria exilis*) straw. *J. Build. Eng.* **2019**, *23*, 250–258. [CrossRef]
18. Turco, C.; Teixeira, M.O.; Teixeira, E.; Mateus, R. Mechanical properties and durability of compressed earth blocks incorporating natural materials. *J. Build. Eng.* **2025**, *111*, 113386. [CrossRef]
19. Schicker, A.; Gier, S. Optimizing the mechanical strength of adobe bricks. *Clays Clay Miner.* **2009**, *57*, 494–501. [CrossRef]
20. Pachamama, R.N.; Faria, P.; Rezende, M.A.P.; Santos Silva, A. Effect of cow dung additions on tropical and Mediterranean earth mortars-mechanical performance and water resistance. *Materials* **2024**, *17*, 2885. [CrossRef]
21. Dormohamadi, M.; Rahimnia, R. Combined effect of compaction and clay content on the mechanical properties of adobe brick. *Case Stud. Constr. Mater.* **2020**, *13*, e00402. [CrossRef]
22. Shetty, R.; Singh, D.N. Utilization of dredged sediments: Contemporary issues. *J. Waterw. Port Coast. Ocean Eng.* **2016**, *142*, 04016025.
23. Zeng, M.; Huang, H.; Zhang, X. Experiment on the performance of recycled powder of construction waste on adobe materials. *Buildings* **2023**, *13*, 1358. [CrossRef]
24. Călătan, G.; Hegyi, A.; Grebenisan, E.; Mircea, A.C. Possibilities of recovery of industrial waste and by-products in adobe-brick-type masonry elements. *Proceedings* **2020**, *63*, 1.
25. Oliveira, C.; Silveira, D.; Varum, H.; Parisi, F.; Miccoli, L.; Solís, M.; Rodríguez-Mariscal, J.D.; Tarque, N. Mechanical characterization of adobe masonry. In *Structural Characterization and Seismic Retrofitting of Adobe Constructions: Experimental and Numerical Developments*; Varum, H., Parisi, F., Tarque, N., Silveira, D., Eds.; Springer: Cham, Switzerland, 2021; pp. 55–92.
26. Eua-apiwatch, S.; Kanjanakijkasem, W. Laboratory study of physical and thermal properties of concrete mixed with Bakelite. *Int. J. GEOMATE* **2023**, *24*, 109–116. [CrossRef]
27. Millogo, Y.; Morel, J.-C.; Aubert, J.-E.; Ghavami, K. Experimental analysis of Pressed Adobe Blocks reinforced with Hibiscus cannabinus fibers. *Constr. Build. Mater.* **2014**, *52*, 71–78. [CrossRef]
28. Mostafa, M.; Uddin, N. Experimental analysis of Compressed Earth Block (CEB) with banana fibers resisting flexural and compression forces. *Case Stud. Constr. Mater.* **2016**, *5*, 53–63. [CrossRef]
29. Polidori, G.; Aras-Gaudry, A.; Beaumont, F.; Bogard, F.; Murer, S.; Lachi, M.; Maalouf, C.; Moussa, T.; Bliard, C.; Fronteau, G.; et al. Adobe bricks of the Champagne region (France): Characterization of a chalky raw earth construction material. *Materials* **2024**, *17*, 2307. [CrossRef] [PubMed]
30. Hejazi, B.; Luz, C.; Grüner, F.; Frick, J.; Garrecht, H. Characterisation of Adobe and Mud–Straw for the Restoration and Rehabilitation of Persian Historical Adobe Buildings. *Materials* **2024**, *17*, 1764. [CrossRef] [PubMed]
31. Bish, D.L.; Post, J.E. Quantitative mineralogical analysis using the Rietveld full-pattern fitting method. *Am. Mineral.* **1993**, *78*, 932–940.
32. Hussain, M.; Levacher, D.; Leblanc, N.; Zmamou, H.; Djeran-Maigre, I.; Razakamanantsoa, A.; Saouti, L. Properties of Mexican tropical palm oil flower and fruit fibers for their prospective use in eco-friendly construction material. *Fibers* **2021**, *9*, 63. [CrossRef]
33. Polidori, G.; Aras-Gaudry, A.; Rousse, C.; Beaumont, F.; Bogard, F.; Murer, S.; Moussa, T.; Bliard, C.; Fronteau, G.; Hamard, E. Analysis of adobes from vernacular raw earth buildings in the Champagne region (France). *Constr. Build. Mater.* **2025**, *470*, 140582. [CrossRef]
34. Calatan, G.; Hegyi, A.; Dico, C.; Mircea, C. Determining the optimum addition of vegetable materials in adobe bricks. *Procedia Technol.* **2016**, *22*, 259–265. [CrossRef]
35. Binici, H.; Aksogan, O.; Shah, T. Investigation of fibre reinforced mud brick as a building material. *Constr. Build. Mater.* **2005**, *19*, 313–318. [CrossRef]
36. Jokhio, G.A.; Al-Tawil, Y.M.Y.; Syed Mohsin, S.M.; Gul, Y.; Ramli, N.I. Compressive and flexural tests on adobe samples reinforced with wire mesh. *IOP Conf. Ser. Mater. Sci. Eng.* **2018**, *318*, 012030. [CrossRef]
37. Hussain, M.; Levacher, D.; Saouti, L.; Leblanc, N.; Zmamou, H.; Djeran-Maigre, I.; Razakamanantsoa, A. Reuse of harbour and river dredged sediments in adobe bricks. *Clean. Mater.* **2022**, *3*, 100046. [CrossRef]
38. Eua-apiwatch, S.; Arjwech, R.; Chairojwattana, A.; Kanjanakijkasem, W.; Kanhari, C.; Pethrung, S. Impact of bentonite content on electrical resistivity and compressive strength of cement paste for grounding system applications. *Eng. Appl. Sci. Res.* **2025**, *52*, 260–269.
39. Christoforou, E.; Kylili, A.; Fokaides, P.A.; Ioannou, I. Cradle to Site Life Cycle Assessment (LCA) of Adobe Bricks. *J. Clean. Prod.* **2016**, *112*, 443–452. [CrossRef]

40. Asdrubali, F.; Grazieschi, G.; Roncone, M.; Thiebat, F.; Carbonaro, C. Sustainability of Building Materials: Embodied Energy and Embodied Carbon of Masonry. *Energies* **2023**, *16*, 1846. [CrossRef]
41. Albuja-Sánchez, J.; Damián-Chalán, A. Leveraging Life Cycle Cost Analysis (LCCA) for Optimized Decision Making in Adobe Construction Materials. *Appl. Sci.* **2024**, *14*, 1760. [CrossRef]